



Highly Concentrated KTFSI: Glyme Electrolytes for K/Bilayered-V₂O₅ Batteries

Xu Liu,^[a, b] Giuseppe Antonio Elia,^{*[a, b]} Xinpei Gao,^[a, b] Bingsheng Qin,^[a, b] Huang Zhang,^[a, b] and Stefano Passerini^{*[a, b]}

Highly concentrated glyme-based electrolytes are friendly to a series of negative electrodes for potassium-based batteries, including potassium metal. However, their compatibility with positive electrodes has been rarely explored. In this work, the influence of the molar fraction of potassium bis(trifluoromethanesulfonyl)imide dissolved in glyme on the cycling ability of K/bilayered-V₂O₅ batteries has been investigated. At high salt concentration, the interaction between K⁺ ions with the glyme is strengthened, leading to a limited number of free glyme molecules. Therefore, the anodic decomposition of the electrolyte solvent, as well as the dissolution of the Al current

collectors, is effectively suppressed, resulting in the improved cycling ability of the K/bilayered-V₂O₅ cells. In these cells, the positive electrode active material exhibits reversible capacities of 93 and 57 mAhg⁻¹ at specific current densities of 50 and 1000 mA g⁻¹, respectively. After 200 charge-discharge cycles at 500 mA g⁻¹, the cell retains 94% of the initial capacity. The promising rate performance and capacity retention demonstrate the importance of proper electrolyte engineering for the K/bilayered-V₂O₅ batteries, and the good compatibility of highly concentrated glyme-based electrolytes with positive electrode materials for potassium batteries.

1. Introduction

The limited supply of cobalt, nickel, and lithium, all being key materials of lithium-ion batteries (LIBs), is pushing the interest towards alternative battery chemistries.^[1,2] Owing to the abundance (and low cost) of the raw materials, potassium batteries (PBs) are receiving a rapidly increasing attention in recent years.^[3,4] Despite the similarity in the chemistry of potassium and lithium,^[5] design and engineering of components for PBs are, however, needed because of the inherent differences between Li⁺ and K⁺ ions, e.g., Lewis acidity and ionic radius. These especially affect the electrolyte, which is an essential component determining the performance of alkali metal and metal-ion batteries (including PBs). Currently, the most commonly used electrolyte for PBs is the solution of potassium hexafluorophosphate in a mixture of ethylene

carbonate and diethyl carbonate (0.8 M KPF₆ in EC:DEC).^[6] However, it has been recently evidenced as DEC is both chemically and electrochemically unstable against the most common anodes (K metal and graphite) for PBs,^[7] leading to poor cell performance. Alternative electrolytes with a new combination of salts and solvents, including high-salt-concentration electrolytes have been reported to improve the stability of K-based cells.^[8-18]

Among them, highly concentrated glyme-based electrolytes are the most versatile ones. For example, Xiao et al. reported the highly concentrated KFSI_{0.5}:glyme enabling reversible potassium plating/stripping with an efficiency of 99%, thanks to the formation of an inorganic compound-rich, solid electrolyte interphase (SEI) on potassium metal.^[16] Notice that plating/stripping efficiency achieved using 0.8 M KPF₆ in EC:DEC is only 50%. Because of the unique SEI formed in highly concentrated KFSI/glyme electrolytes, enhanced cycling ability of perylene-3,4,9,10-tetracarboxylic dianhydride,^[10] Bi-Sb alloy,^[18] and graphite^[14] electrodes has been achieved. Similar behavior was also observed for WS₂ and bismuth electrodes in highly concentrated KTFSI/tetraglyme electrolytes.^[8,14]

So far, the investigation has focused on negative electrode materials.^[19,20] In fact, numerous anode materials with high stability, capacity, and rate performance have been developed, such as carbonaceous materials,^[21,22] transitional-metal dichalcogenides,^[23-25] alloy materials,^[26,27] phosphides,^[11,28] and organic compounds.^[10,29] On the other hand, the choice of positive electrode materials for PBs is very limited due to, among other reasons, the sluggish insertion kinetics resulting from the large K⁺ ionic radius. With its interlayer distance above 10 Å,^[30] bilayered-V₂O₅ appears to be a promising host for the large K⁺. However, this material faces severe capacity fading upon cycling in carbonate-based electrolytes.^[31] In our

[a] X. Liu, Dr. G. A. Elia, Dr. X. Gao, Dr. B. Qin, Prof. Dr. H. Zhang, Prof. Dr. S. Passerini
Helmholtz Institute Ulm (HIU) Electrochemical Energy Storage
Helmholtzstrasse 11, 89081 Ulm, Germany
E-mail: giuseppe.elia@kit.edu
stefano.passerini@kit.edu

[b] X. Liu, Dr. G. A. Elia, Dr. X. Gao, Dr. B. Qin, Prof. Dr. H. Zhang, Prof. Dr. S. Passerini
Karlsruhe Institute of Technology (KIT)
PO Box 3640, D-76021 Karlsruhe, Germany

Supporting information for this article is available on the WWW under <https://doi.org/10.1002/batt.202000003>

This publication is part of a joint Special Issue with ChemSusChem focusing on "2D Energy Storage Materials"

© 2020 The Authors. Published by Wiley-VCH Verlag GmbH & Co. KGaA. This is an open access article under the terms of the Creative Commons Attribution Non-Commercial NoDerivs License, which permits use and distribution in any medium, provided the original work is properly cited, the use is non-commercial and no modifications or adaptations are made.

previous work, we demonstrated that the lifespan of Li/bilayered- V_2O_5 and Na/bilayered- V_2O_5 batteries is effectively improved through the replacement of the traditional carbonate-based electrolytes with ionic liquid- and glyme-based electrolytes, respectively.^[32,33] It was also proved that the cycling stability of the Na/electrolyte interface plays a critical role in the performance of Na/bilayered- V_2O_5 batteries.^[33]

Herein, K/bilayered- V_2O_5 batteries are realized and tested using highly concentrated, glyme-based electrolytes. In particular, the influence of the KTFSI:glyme molar ratio on the solvent-ion interactions, physical properties, anodic electrochemical stability window, and anodic dissolution of Al current collectors is systemically investigated. The compatibility of the KTFSI_x:glyme electrolytes with K/bilayered- V_2O_5 batteries is also evaluated.

2. Results and Discussion

The solvent-ion interactions occurring in the KTFSI_x:glyme ($x = 0.08, 0.15, 0.30, \text{ and } 0.45$) electrolytes are characterized via

Raman spectroscopy. The broad peak at $735\text{--}750\text{ cm}^{-1}$ (Figure 1(a)) can be assigned to the TFSI⁻ vibration.^[34] The peak shifts toward high wavenumbers with higher salt concentration, indicating for the stronger involvement of TFSI⁻ in the K⁺ coordination. Also, a series of peaks is observed in the $805\text{--}890\text{ cm}^{-1}$ range (Figure 1(b)), reflecting the vibrations of the glyme molecules. The pure glyme shows two peaks centered at 821 cm^{-1} (Peak I) and 850 cm^{-1} (Peak III), corresponding to the CH₂ rocking and C–O stretching, respectively. The addition of KTFSI, however, introduces two new bands at 835 cm^{-1} (Peak II) and 860 cm^{-1} (Peak IV).^[35] The latter one originates from the C–O coordinated with K⁺, while the former can be attributed to the shift of Peak I by the coordinated C–O, since CH₂ is unlikely to participate in the coordination of K⁺. Upon increasing the KTFSI molar ratio, peaks I and III gradually decline while peaks II and IV increases, evidencing the decrease of free glyme molecules. The average number of glyme molecules coordinating each K⁺ ion (n) is expected to change because of the increasing K content. Based on the area of peaks III and IV, n can be calculated according to Equation (1).^[34]

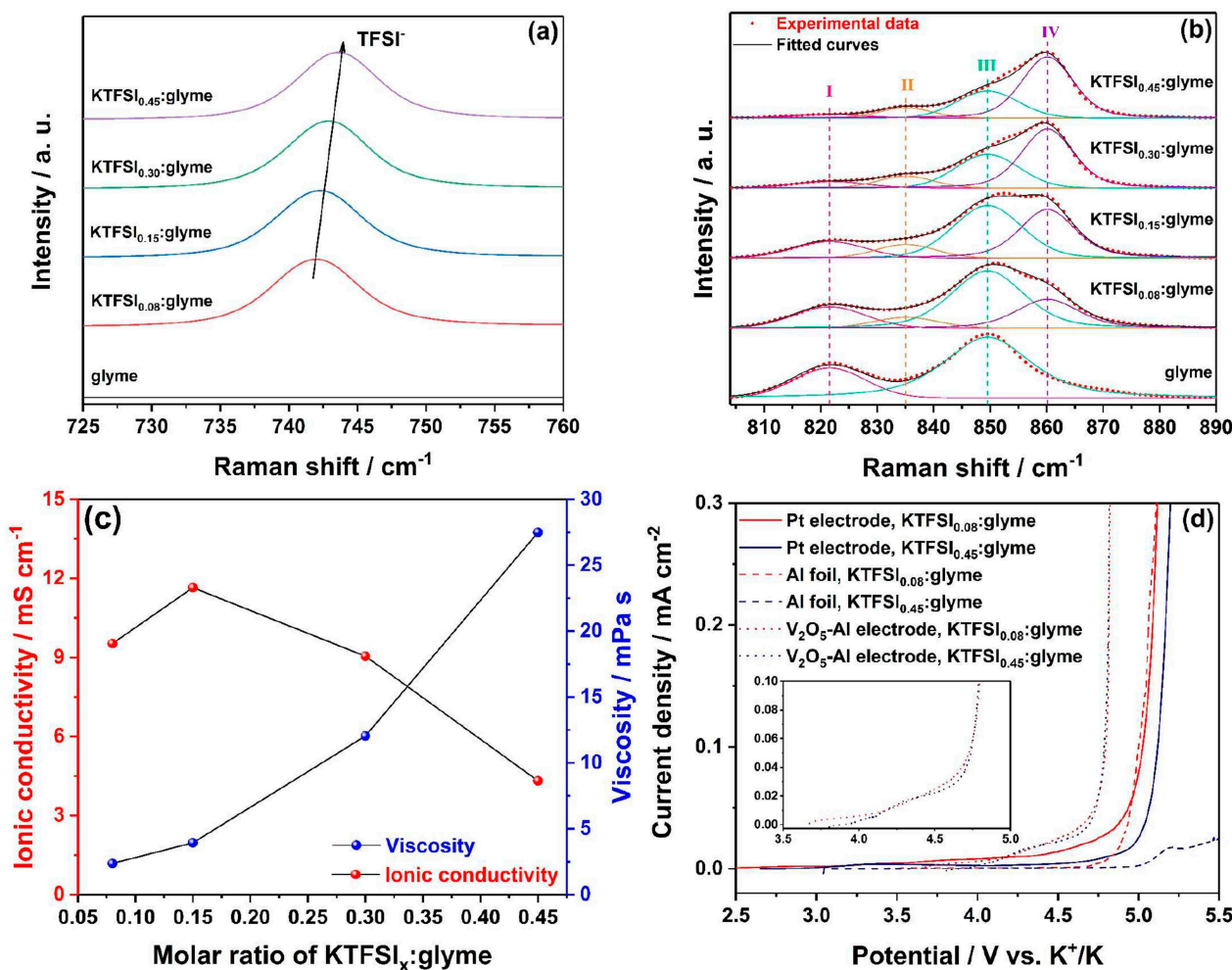


Figure 1. Raman spectra of as-prepared KTFSI_x:glyme electrolytes with different salt concentrations: (a) vibration of TFSI⁻ and (b) CH₂ rocking and C–O stretching from glyme molecules. (c) Ionic conductivity and viscosity of as-prepared KTFSI_x:glyme electrolytes at 20 °C. (d) Linear sweep voltammograms of KTFSI_{0.08}:glyme and KTFSI_{0.45}:glyme using different working electrodes with a scan rate of 0.2 mV s⁻¹.

$$n = \frac{f_{\text{coordinated glyme}}}{x} = \frac{A_{\text{IV}}/(A_{\text{III}} + A_{\text{IV}})}{x} \quad (1)$$

Where $f_{\text{coordinated glyme}}$ is the fraction of coordinated glyme molecules, x is the molar fraction of KTFSI in the electrolyte, and A_{III} and A_{IV} are the areas of peak III and IV, respectively. The resulting values of n for the KTFSI $_x$:glyme electrolytes are 4.1, 3.5, 2.7, and 2.2 for $x=0.08$, 0.15, 0.30, and 0.45, respectively. This means that, practically, all glymes molecules are involved in the K⁺ ion coordination at the highest salt concentration ($x=0.45$). Even in the KTFSI $_{0.3}$:glyme electrolyte only a few free glyme molecules exist. This is obviously resulting in the increasing coordination of the K⁺ ions by the TFSI⁻ anion, consistent with the shift of the TFSI⁻ band (Figure 1a).

Figure 1(c) displays the viscosity and ionic conductivity of the various KTFSI $_x$:glyme electrolytes at 20 °C. The specific values can be found in Table S1. As expected, the viscosity of the electrolyte rises upon increasing salt concentrations.^[36] However, the ionic conductivity shows a maximum for $x=0.15$. Such a bell-shape trend is frequently observed upon increasing salt concentration in electrolytes due to the opposite effects of the increasing number of charge carriers counter-balanced by increased viscosity and ion-pairing. For molar ratios up to 0.15, the increasing concentration results into the increase of dissociated free ions, i.e., the charge carriers, thus improving the ionic conductivity. For higher molar fractions, however, the increase of viscosity and ion-pairs/aggregates result in lower ionic conductivities.^[37] Nevertheless, the KTFSI $_{0.45}$:glyme electrolyte still meets a conductivity value ($10^{-3} \text{ S cm}^{-1}$) feasible for practical applications. In fact, although the KTFSI $_{0.45}$:glyme viscosity is as high as 27.5 mPa s, which could cause difficulties for the electrode wetting, much higher values have been reported for other highly concentrated electrolytes for LIBs.^[38,39] For example, the viscosity of highly concentrated 5.5 M LiFSA/DMC at 30 °C is as high as 240 mPa s.^[40] Therefore, the highly concentrated KTFSI $_x$:glyme electrolytes appear to be acceptable for use as electrolytes in PBs in terms of viscosity and ionic conductivity.

Figure 1(d) displays the linear sweep voltammograms of the most diluted (KTFSI $_{0.08}$:glyme) and concentrated (KTFSI $_{0.45}$:glyme) electrolytes using different working electrodes. In general, a lower extent of the anodic electrochemical oxidation is observed for the highly concentrated electrolyte. This is certainly attributable to the decreased amount of free glyme, which is known to have poor anodic stability.^[35] However, it is also observed that the onset of the oxidation process varies with different electrodes. When the conventional Pt electrode is replaced with the Al electrode (which is commonly used as current collector), the anodic decomposition of the electrolyte is effectively suppressed, especially for the highly concentrated electrolyte. The anodic current detected using KTFSI $_{0.45}$:glyme is only $0.0025 \text{ mA cm}^{-2}$ at 5.0 V (vs. K⁺/K). Even with the diluted electrolyte (KTFSI $_{0.08}$:glyme), the anodic current is lower than 0.002 mA cm^{-2} up to 4.6 V vs. K⁺/K. However, the anodic decomposition of the electrolytes is somehow catalytically enhanced by the presence of vanadium

oxide. Nonetheless, the anodic current recorded with both the diluted and concentrated electrolytes does not show a large increase up to 4.7 V vs. K⁺/K; the KTFSI $_{0.45}$:glyme electrolyte is still the most stable, as shown in the inset of Figure 1(d).

The LSV measurements in Figure 1(d) also suggest for the stability of the Al current collector towards anodic dissolution in the KTFSI $_x$:glyme electrolytes, even for low salt concentration. However, to verify the long-term behavior, repeated cyclic voltammetry (CV) tests were applied with a scan rate of 1 mV s^{-1} . A few, selected CV curves are displayed in Figure 2 together with the SEM images of the Al current collectors taken at the end of the test, i.e., after 50 cycles. No dramatic current increase is detected upon cycling, which is in agreement with the LSV results. However, the anodic current changes depending on the electrolyte composition. After 50 cycles in KTFSI $_{0.08}$:glyme, distinct pitting dissolution of the Al foil is observed, as shown in Figure 2(b). When KTFSI $_{0.45}$:glyme is used instead, the anodic current is evidently lower and the SEM image of the Al foil does not evidence any major difference with respect to the pristine foil (Figure S1). Nonetheless, if the upper cut-off is increased to 4.2 V (vs. K⁺/K), the CV curves display increased current flow accompanied by the dissolution of Al (see Figure 2(e) and (f), respectively). These results demonstrate that high KTFSI concentrations indeed enhance the stability of Al towards anodic dissolution, although to a lower extent than that indicated by the LSV measurements. Such an enhancement is tightly associated with the KTFSI content in the electrolyte.^[41] In fact, a surface layer of Al(TFSI) $_3$ may form on the Al electrode, preventing further anodic dissolution.^[42-44] This, however, does not occur when free glyme molecules are present in the electrolyte, leading to the continuous Al dissolution from the current collector. On the other hand, the limited number of free glyme available in the concentrated electrolyte results in the precipitation of Al(TFSI) $_3$ on the Al, inhibiting its further anodic dissolution.

To verify the compatibility of the glyme-based electrolytes with PBs, coin cells were assembled using metallic potassium as the negative electrode, and bilayered-V $_2$ O $_5$ electrodes as positive electrodes. The evolution of the specific capacity of bilayered V $_2$ O $_5$ and Coulombic efficiency measured at 500 mA g^{-1} within 1.5–3.8 V is shown in Figure 3(a) and (b), respectively. The salt concentration shows significant influence on both the specific capacity and the cycling ability. High salt concentrations lead to slightly lower initial specific capacities, which are largely attributed to their high viscosity and low ionic conductivity. On the other hand, the concentrated electrolytes promote the cycling ability of the cell. In fact, with the diluted KTFSI $_x$:glyme ($0.08 \leq x \leq 0.30$) electrolytes, the cell capacity always fades almost completely although within a different number of cycles (max. 170), in turn depending on the K-salt content. The cell employing KTFSI $_{0.45}$:glyme, however, offers a capacity retention of 94% after 200 cycles, which is substantially better than that of the cell employing the conventional (0.8 M KPF $_6$ in EC/DEC) carbonate electrolyte, as shown in Figure 3a. This result confirms the feasible use of KTFSI $_{0.45}$:glyme as electrolyte for K/bilayered-V $_2$ O $_5$ batteries. Notice that the capacity fading observed in the diluted

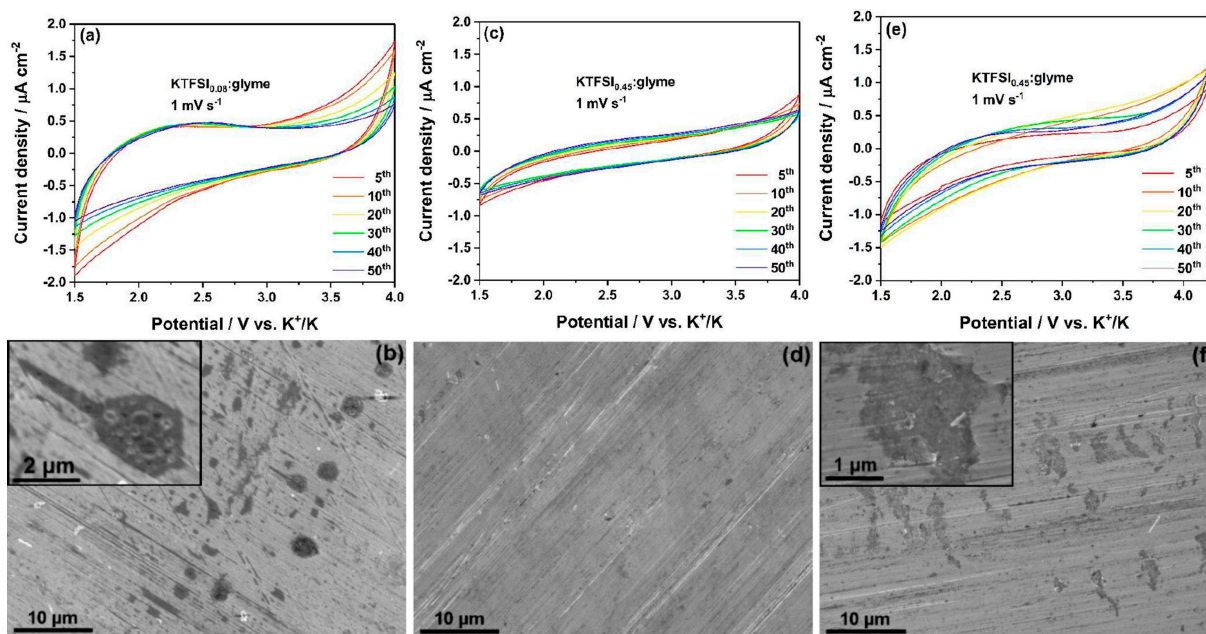


Figure 2. Cyclic voltammograms (1 mV s^{-1}) of Al foils in different electrolytes and potential windows at selected cycles: (a) $\text{KTFSI}_{0.08}:\text{glyme}$, 1.5–4.0 V vs. K^+/K ; (c) $\text{KTFSI}_{0.45}:\text{glyme}$, 1.5–4.0 V vs. K^+/K ; (e) $\text{KTFSI}_{0.45}:\text{glyme}$, 1.5–4.2 V vs. K^+/K . SEM images of the Al foils after 50 cycles in the different electrolytes and potential windows: (b) $\text{KTFSI}_{0.08}:\text{glyme}$, 1.5–4.0 V vs. K^+/K ; (d) $\text{KTFSI}_{0.45}:\text{glyme}$, 1.5–4.0 V vs. K^+/K ; (f) $\text{KTFSI}_{0.45}:\text{glyme}$, 1.5–4.2 V vs. K^+/K .

$\text{KTFSI}_x:\text{glyme}$ electrolytes is also accompanied with a decrease in Coulombic efficiency, indicating the presence of side reactions. On the other hand, the cell employing $\text{KTFSI}_{0.45}:\text{glyme}$ offers a Coulombic efficiency always higher than 99.5%, which is a rather high value considering the use of the potassium metal electrode.

The extent of the irreversible side reactions, also responsible for the fast capacity fading, occurring with the diluted $\text{KTFSI}_x:\text{glyme}$ electrolytes is clearly seen in Figure 3(c), in which the voltage profile of all cells at the 35th cycle is compared. With the exception of the cell employing $\text{KTFSI}_{0.45}:\text{glyme}$, all other cells showed charge capacities much higher than the corresponding discharge capacities, evidencing the occurrence of irreversible side reactions. Since the intercalation (and deintercalation) of potassium ions in bilayered- V_2O_5 occurs via the solid solution processes, only one phase exists. Thus, the charge-discharge profiles do not show any plateau, well obeying the Gibbs phase rule.^[33] The corresponding differential capacity plots, Figure 3(d), evidence irreversible anodic peaks in the high voltage region ($> 3 \text{ V}$), with the exception of the cell employing $\text{KTFSI}_{0.45}:\text{glyme}$. Such irreversible peaks well match the electrolyte decomposition and Al anodic dissolution phenomena, as shown in Figure 1(d) and Figure 2, respectively. Hence, it is reasonable to infer that the electrolyte decomposition and Al dissolution are mainly responsible for the irreversible reactions observed in diluted $\text{KTFSI}_x:\text{glyme}$ electrolytes.

Because of the poor performance of the diluted electrolytes, only K/bilayered- V_2O_5 cells employing $\text{KTFSI}_{0.45}:\text{glyme}$ were realized and investigated. First, the effect of the upper cut-off voltage upon galvanostatic cycling on the rate performance and cycling ability of K/bilayered- V_2O_5 cells was evaluated.

Figure 4(a) compares the specific capacity and Coulombic efficiency of a few cells cycled using different upper cut-off voltages and specific currents. As expected, increasing the upper cut-off voltage leads to an increase of the delivered specific capacity. For example, the specific capacity recorded at 200 mA g^{-1} increases from 70 to 84, and 111 mA h g^{-1} for the upper cut off voltage increasing from 3.8 V to 4.0 and 4.2 V, respectively. However, the highest upper cut-off leads to decreased Coulombic efficiency, which is only 92.57% at the 100th cycle. This implies that the irreversible side reactions, i.e., electrolyte decomposition and Al dissolution, also occur with $\text{KTFSI}_{0.45}:\text{glyme}$ at rather high cell voltages. Hence, the 1.5–4.0 V is taken as the optimal voltage window for the K/bilayered- V_2O_5 cells. Additionally, the charge-discharge voltage profiles at different specific currents within this voltage window, Figure 4(b), demonstrate the good rate performance of the cell. In fact, while the reversible capacity is 93 mA h g^{-1} upon cycling at 50 mA g^{-1} , 57 mA h g^{-1} are still retained at the highest specific current used (1 A g^{-1}).

The long-term cycling ability of cells operating within upper cut-off voltages of 4.0 and 4.2 V is displayed in Figure 4(c). Within the 1.5–4.2 V window the cell exhibits an initial activation process, delivering a capacity from 74 mA h g^{-1} to 109 mA h g^{-1} at the 78th cycle. After, the capacity decreases while the Coulombic efficiency varies somehow randomly, which is typically associated with dendrite evolution at the metal (K) electrode. At the 200th cycle, the capacity is 82.8 mA h g^{-1} , corresponding to 76% of the maximum capacity. However, for the cell cycled in the 1.5–4.0 V window, the capacity evolution within the 200 cycles is quite smooth and flat while the Coulombic efficiency stays above 98.5%, except for the last few cycles. The reversible capacity gradually

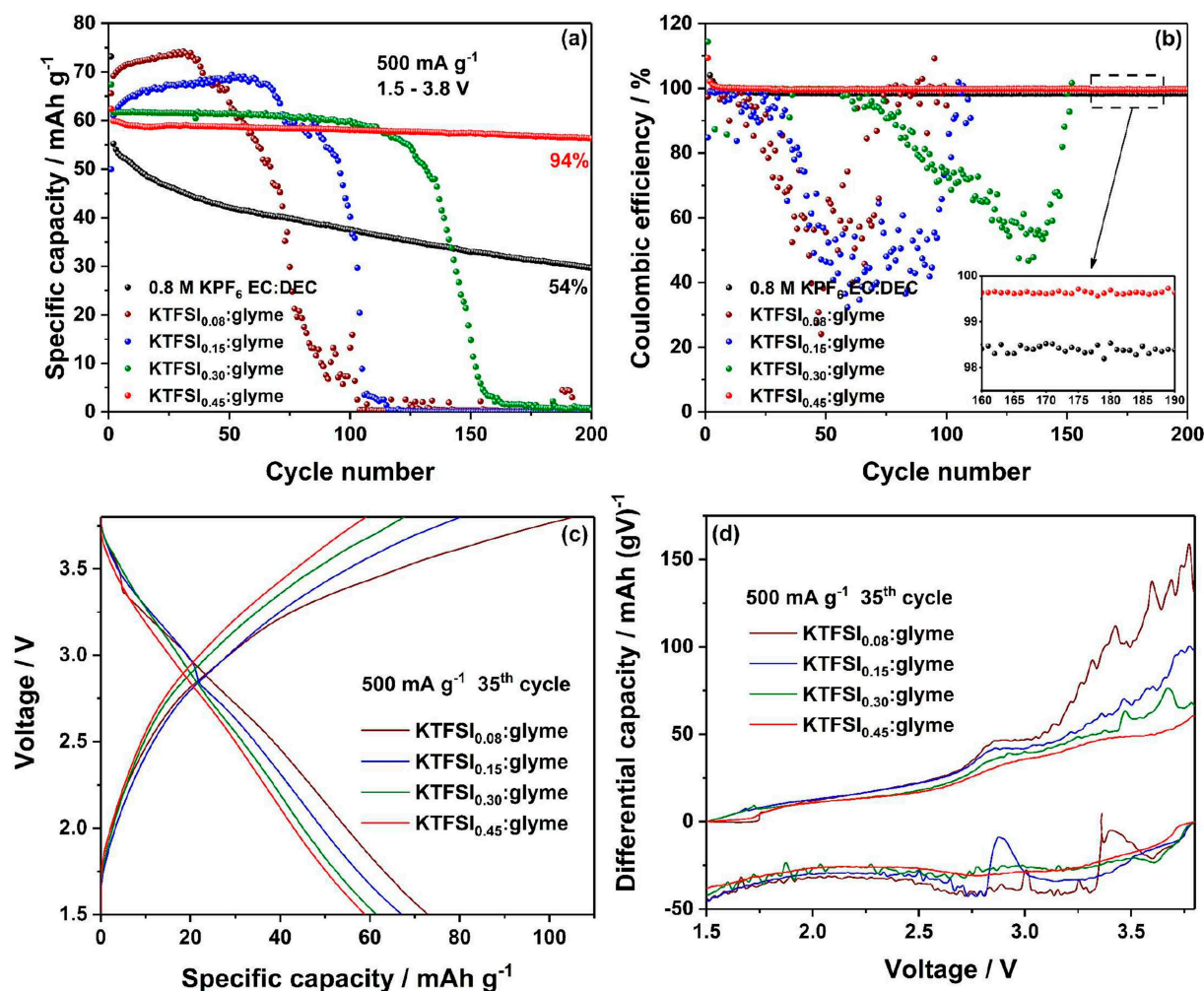


Figure 3. Evolution of (a) discharge specific capacity and (b) Coulombic efficiency of the K/bilayered- V_2O_5 cells using the various electrolytes (see legends) upon cycling ability tests at 500 mA g^{-1} within the 1.5–3.8 V voltage window. (c) The charge-discharge profiles and (d) corresponding differential capacity plots of the cells using the four $KTFSI_x$:glyme electrolytes at the 35th cycle.

increases from 66 mAh g^{-1} to 72 mAh g^{-1} at the 40th cycle. After 160 cycles, 66 mAh g^{-1} are still retained, corresponding to 92% of the maximum capacity at the 40th cycle. The charge-discharge profiles of selected cycles are displayed in Figure 4 (d). After the 1st cycle, the voltage curves overlap well with each other, indicating for the good cyclability and stability of the K/bilayered- V_2O_5 cell employing $KTFSI_{0.45}$:glyme as the electrolyte.

3. Conclusions

The characterization of $KTFSI_x$:glyme electrolytes shows that the strengthened interaction between K^+ and $TFSI^-$ as well as glyme molecules upon increasing K-salt concentrations leads to reduced free glyme molecules. The resulting change of the electrolyte structure leads to its improved electrochemical stability window and compatibility with the Al current collector, eventually resulting in the rather promising cycling ability of the K/bilayered- V_2O_5 employing the $KTFSI_{0.45}$:glyme. With such

an electrolyte, the upper cut-off cell voltage of 4 V enables promising specific capacities, rate performance and cycling ability, highlighting the importance of “electrolyte engineering” as well as the good compatibility of the highly concentrated glyme-based electrolytes within PBs.

Experimental Section

Preparation of the electrolytes

The electrolyte preparation was carried out in an Ar-filled glove box with H_2O and O_2 levels < 0.1 ppm. Potassium bis(trifluoromethanesulfonyl)imide ($KTFSI$, Solvionic, 99.5%) and potassium hexafluorophosphate (KPF_6 , Sigma-Aldrich, 99%) were dried at 120°C under vacuum (1×10^{-3} bar) for 12 h. The 1,2-dimethylglycol (glyme, Sigma-Aldrich, anhydrous, 99.5%) was dried using molecular sieves (Merck, 3 Å) for 3 days to remove residual water in the solvent. Ethylene carbonate (EC, 99.95%, BASF) and diethyl carbonate (DEC, battery grade, UBE) were used as received. The solid particles in the electrolytes were filtered via syringe filters (LLG, PTFE, 0.2 μm). The $KTFSI_x$:glyme ($x = 0.08, 0.15, 0.30, \text{ and } 0.45$)

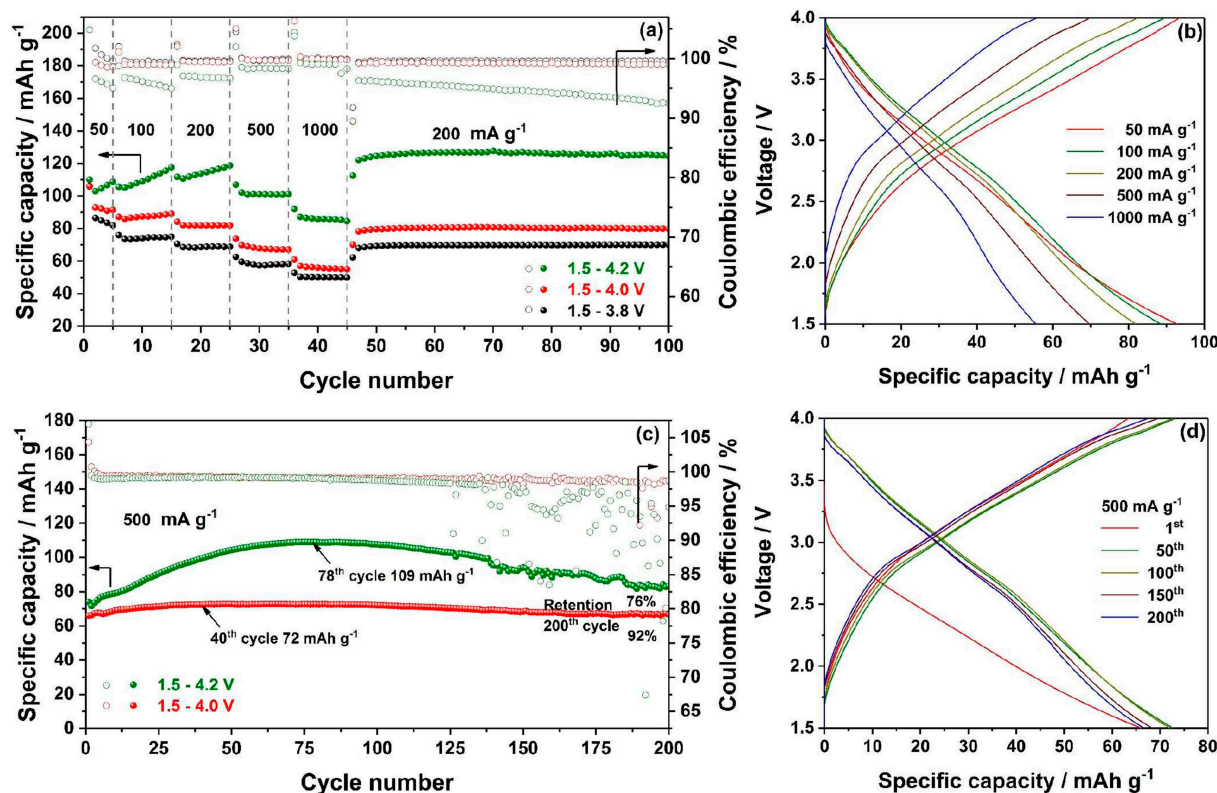


Figure 4. Electrochemical performance of K/bilayered- V_2O_5 cells with $KTFSl_{0.45}$:glyme electrolyte. (a) Charge-discharge profiles of the cell operating within 1.5–4.0 V at different specific currents. (b) Rate performance of the cell with different voltage windows. (c) The charge-discharge curves of the cell operating within 1.5–4.0 V at selected cycles upon the cycling ability test. (d) Specific capacity and Coulombic efficiency of the cells using different voltage windows upon cycling at 500 mA g^{-1} .

electrolytes were prepared by stirring the appropriate amount of KTFSl in the glyme. The commonly used 0.8 M KPF_6 in EC/DEC (1:1 in volume ratio) was also prepared analogously.

Synthesis of bilayered- V_2O_5 and fabrication of the electrodes

The bilayered- V_2O_5 composite containing 5 wt.% GO was used to investigate the influence of KTFSl-Glyme based electrolytes on the potassium storage properties of bilayered- V_2O_5 . The composite was prepared via a microwave-assisted hydrothermal method, which has been reported elsewhere.^[33] Its preparation procedure, structure, composition, morphology, and texture properties can be found in that work. The electrodes were fabricated in the dry room by doctor-blade casting of slurries on aluminum foil (current collector). The slurry was composed of 70 wt.% active material, 20 wt.% carbon black (Super C65, IMERYS), and 10 wt.% polyacrylic acid (Sigma-Aldrich, average $M_w \sim 1250000$) binder dispersed/dissolved in ethanol (Merck Millipore, ethanol absolute). After the evaporation of ethanol in the dry room, electrodes with a diameter of 12 mm were punched and further dried at 150°C under vacuum (1×10^{-3} bar) for 12 h. The average active material (V_2O_5 /GO) mass loading was 1.0 mg cm^{-2} .

Physico-chemical characterization

The Raman measurements were recorded on a RAM II FT-Raman module of a Bruker Vertex70 FT-IR spectrometer with a laser wavelength of 1064 nm and laser power of 300 mW. The collected spectra are the average of 500 scans at an optical resolution of 2 cm^{-1} . The samples were sealed in NMR glass tubes in an argon-

filled glove box. Conductivities were determined via electrochemical impedance spectroscopy (EIS, Mmates-Biologic) by means of sealed Pt-black/Pt-black cells (Mmates). The cell constants were determined using a 0.01 M KCl standard solution (Fluka). The viscosity of the electrolytes was tested in a dry room environment by means of an Anton-Paar Physica MCR102 rheometer, applying constant shear rates, and using a Peltier system for cooling/heating. The conductivity and viscosity measurements were carried out at 20°C . Scanning electron microscopy (SEM) images were obtained using a Zeiss LEO 1550 microscope. The Al foils, taken from cycled cells, were washed with dimethyl carbonate (DMC, battery grade, UBE), dried, and then transferred to the SEM chamber via a sealed transfer box.

Electrochemical measurements

The cell assembly was carried out in an Ar-filled glove box with H_2O and O_2 levels $< 0.1 \text{ ppm}$. To investigate the electrochemical anodic stability and corrosion effect of the electrolytes, three electrode Swagelok-type cells were assembled using potassium metal (99.5%, Sigma-Aldrich) as the counter and reference electrodes, and glass fiber disk (Whatman GF/F) as separator. The electrochemical anodic stability of the electrolytes was assessed via linear sweep voltammetry (LSV) at 0.2 mV s^{-1} . Three different electrodes, including Pt microelectrode (0.79 mm^2), Al foil (1.13 cm^2), and as-fabricated bilayered- V_2O_5 electrode (1.13 cm^2) were separately used as working electrodes to evaluate their influence on the electrochemical anodic stability of the electrolyte. The corrosion effect of electrolytes on the Al foil was evaluated through cyclic voltammetry measurements with Al foils (1.13 cm^2)

as working electrodes. Both the CV and LSV measurements were operated via the galvanostat/potentiostat VMP2 (Bio-Logic, France). CR2032-type coin cells were assembled to evaluate the electrochemical performance of the bilayered-V₂O₅ electrodes in different electrolytes, using potassium metal as counter electrode and glass fiber disk (Whatman GF/F) as separator. In every cell setup, 120 μL of electrolyte was used. Their rate performance and cycling ability were tested via the MACCOR series 4000 battery cyclers. The specific currents and specific capacities of K/bilayered-V₂O₅ cells refer to the weight of the positive electrode material only.

Acknowledgements

X.L., B.Q., and H.Z. gratefully acknowledge financial support from the China Scholarship Council (CSC). Financial support from the support Initiative and Networking Fund of the Helmholtz Association within the Network of Excellence on post-Lithium batteries (ExNet-0035) is also acknowledged.

Keywords: potassium batteries · highly concentrated electrolytes · glyme · KTFSI · vanadium oxide · bilayered-V₂O₅

- [1] A. Moretti, F. Maroni, I. Osada, F. Nobili, S. Passerini, *ChemElectroChem* **2015**, *2*, 529–537.
- [2] C. Vaalma, D. Buchholz, M. Weil, S. Passerini, *Nat. Rev. Mater.* **2018**, *3*, 18013.
- [3] J. Y. Hwang, S. T. Myung, Y. K. Sun, *Adv. Funct. Mater.* **2018**, *28*, 1802938.
- [4] Y. S. Xu, S. Y. Duan, Y. G. Sun, D. S. Bin, X. S. Tao, D. Zhang, Y. Liu, A. M. Cao, L. J. Wan, *J. Mater. Chem. Chron. A* **2019**, *7*, 4334–4352.
- [5] T. Deng, X. L. Fan, C. Luo, J. Chen, L. Chen, S. Hou, N. Eidson, X. Q. Zhou, C. S. Wang, *Nano Lett.* **2018**, *18*, 1522–1529.
- [6] H. Kim, J. C. Kim, M. Bianchini, D. H. Seo, J. Rodriguez-Carria, G. Ceder, *Adv. Energy Mater.* **2018**, *8*, 1702384.
- [7] Y. Lei, L. Qin, R. L. Liu, K. C. Lau, Y. Y. Wu, D. Y. Zhai, B. H. Li, F. Y. Kang, *ACS Appl. Energy Mater.* **2018**, *1*, 1828–1833.
- [8] R. D. Zhang, J. Z. Bao, Y. L. Pan, C. F. Sun, *Chem. Sci.* **2019**, *10*, 2604–2612.
- [9] B. F. Li, J. Zhao, Z. H. Zhang, C. Zhao, P. F. Sun, P. X. Bai, J. X. Yang, Z. Zhou, Y. H. Xu, *Adv. Funct. Mater.* **2019**, *29*, 1807137.
- [10] L. Fan, R. F. Ma, J. Wang, H. G. Yang, B. G. Lu, *Adv. Mater.* **2018**, *30*, 1805486.
- [11] W. C. Zhang, Z. B. Wu, J. Zhang, G. P. Liu, N. H. Yang, R. S. Liu, W. L. Pang, W. W. Li, Z. P. Guo, *Nano Energy* **2018**, *53*, 967–974.
- [12] J. M. Ge, L. Fan, J. Wang, Q. F. Zhang, Z. M. Liu, E. J. Zhang, Q. Liu, X. Z. Yu, B. G. Lu, *Adv. Energy Mater.* **2018**, *8*, 1801477.
- [13] T. Hosaka, K. Kubota, H. Kojima, S. Komaba, *Chem. Commun.* **2018**, *54*, 8387–8390.
- [14] R. D. Zhang, J. Z. Bao, Y. H. Wang, C. F. Sun, *Chem. Sci.* **2018**, *9*, 6193–6198.
- [15] Q. Zhang, J. F. Mao, W. K. Pang, T. Zheng, V. Sencadas, Y. Chen, Y. J. Liu, Y. P. Guo, *Adv. Energy Mater.* **2018**, *8*, 1703288.
- [16] N. Xiao, W. D. McCulloch, Y. Y. Wu, *J. Am. Chem. Soc. Rev.* **2017**, *139*, 9475–9478.
- [17] J. Zheng, Y. Yang, X. L. Fan, G. B. Ji, X. Ji, H. Y. Wang, S. Hou, M. R. Zachariah, C. S. Wang, *Energy Environ. Sci.* **2019**, *12*, 615–623.
- [18] J. Wang, L. Fan, Z. M. Liu, S. H. Chen, Q. F. Zhang, L. L. Wang, H. Q. Yang, X. Z. Yu, B. G. Lu, *ACS Nano* **2019**, *13*, 3703–3713.
- [19] T. Dong, X. L. Fan, C. Luo, J. Chen, L. Chen, S. Hou, N. Eidson, X. Q. Zhou, C. S. Wang, *Nano Lett.* **2018**, *18*, 1522–1529.
- [20] Y. H. Pei, C. N. Mu, H. X. Li, F. J. Li, J. Chen, *ChemSusChem* **2018**, *11*, 1285–1289.
- [21] B. Cao, Q. Zhang, H. Liu, B. Xu, S. L. Zhang, T. F. Zhou, J. F. Mao, W. K. Pang, Z. P. Guo, A. Li, J. S. Zhou, X. H. Chen, H. H. Song, *Adv. Energy Mater.* **2018**, *8*, 1801149.
- [22] D. P. Li, X. H. Ren, Q. Ai, Q. Sun, L. Zhu, Y. Liu, Z. Liang, R. Q. Peng, P. C. Si, J. Lou, J. K. Feng, L. J. Ci, *Adv. Energy Mater.* **2018**, *8*, 1802386.
- [23] H. W. Huang, J. Cui, G. X. Liu, R. Bi, L. Zhang, *ACS Nano* **2019**, *13*, 3448–3456.
- [24] B. R. Jia, Q. Y. Yu, Y. Z. Zhao, M. L. Qin, W. Wang, Z. W. Liu, C. Y. Lao, Y. Liu, H. W. Wu, Z. L. Zhang, X. H. Qu, *Adv. Funct. Mater.* **2018**, *28*, 1803409.
- [25] C. M. Chen, Y. C. Yang, X. Tang, R. H. Qiu, S. Y. Wang, G. Z. Cao, M. Zhang, *Small* **2019**, *15*, 1804740.
- [26] H. Wang, L. F. Wang, L. C. Wang, Z. Xing, X. Wu, W. Zhao, X. J. Qi, Z. C. Ju, Q. C. Zhuang, *Chem. Eur. J.* **2018**, *24*, 13897–13902.
- [27] K. X. Lei, C. C. Wang, L. J. Liu, Y. W. Luo, C. N. Mu, F. J. Li, J. Chen, *Angew. Chem. Int. Ed.* **2018**, *57*, 4687–4691; *Angew. Chem.* **2018**, *130*, 4777–4781.
- [28] J. Bai, B. J. Xi, H. Z. Mao, Y. Lin, X. J. Ma, J. K. Feng, S. L. Xiong, *Adv. Mater.* **2018**, *30*, 1802310.
- [29] K. X. Lei, F. J. Li, C. N. Mu, J. B. Wang, Q. Zhao, C. C. Chen, J. Chen, *Energy Environ. Sci.* **2017**, *10*, 552–557.
- [30] Y. Q. Yang, Y. Tang, G. Z. Fang, L. T. Shan, J. S. Guo, W. Y. Zhang, C. Wang, L. B. Wang, J. Zhou, S. Q. Liang, *Energy Environ. Sci.* **2018**, *11*, 3157–3162.
- [31] B. B. Tian, W. Tang, C. L. Su, Y. Li, *ACS Appl. Mater. Interfaces* **2018**, *10*, 642–650.
- [32] A. Moretti, S. Jeong, S. Passerini, *ChemElectroChem* **2016**, *3*, 1048–1053.
- [33] X. Liu, B. S. Qin, H. Zhang, A. Moretti, S. Passerini, *ACS Appl. Energy Mater.* **2019**, DOI: 10.1021/acsaem.9b00128.
- [34] X. P. Gao, A. Mariani, S. Jeong, X. Liu, X. W. Dou, M. Ding, A. Moretti, S. Passerini, *J. Power Sources* **2019**, *423*, 52–59.
- [35] Y. Yamada, M. Yaegashi, T. Abe, A. Yamada, *Chem. Commun.* **2013**, *49*, 11194–11196.
- [36] C. X. Geng, D. Buchholz, G. T. Kim, D. V. Carvalho, H. Zhang, L. G. Chagas, S. Passerini, *Small Methods* **2019**, *3*, 1800208.
- [37] Y. Yamada, A. Yamada, *J. Electrochem. Soc.* **2015**, *162*, A2406–A2423.
- [38] Y. Yamada, J. H. Wang, S. Ko, E. Watanabe, A. Yamada, *Nat. Energy* **2019**, *4*, 269–280.
- [39] X. P. Gao, F. L. Wu, A. Mariani, S. Passerini, *ChemSusChem* **2019**, *12*, 1–10.
- [40] J. H. Wang, Y. Yamada, K. Sodeyama, C. H. Chiang, Y. Tateyama, A. Yamada, *Nat. Commun.* **2016**, *7*, 12032.
- [41] Y. Yamada, C. H. Chiang, K. Sodeyama, J. H. Wang, Y. Tateyama, A. Yamada, *ChemElectroChem* **2015**, *2*, 1687–1694.
- [42] R. S. Kühnel, M. Lübke, M. Winter, S. Passerini, A. Balducci, *J. Power Sources* **2012**, *214*, 178–184.
- [43] R. S. Kühnel, J. Reiter, S. Jeong, S. Passerini, A. Balducci, *Electrochem. Commun.* **2014**, *38*, 117–119.
- [44] R. S. Kühnel, N. Böckenfeld, S. Passerini, M. Winter, A. Balducci, *Electrochim. Acta* **2011**, *56*, 4092–4099.

Manuscript received: January 2, 2020
Accepted manuscript online: January 4, 2020
Version of record online: January 22, 2020